TABLE 3. **Peak CSF S100B and cytokine concentrations in the TBI patients per outcome**

| | S100B (μg/L) | IL-1β (pg/mL) | TNFα (pg/mL) | IL-6 (pg/mL) | IL-8 (pg/mL) | IL-10 (pg/mL) |
|---|---|---|---|---|---|---|
| Unfavorable* (n = 8) | 1231 ± 378 | 14.8 ± 3.4 | 12.1 ± 2.0 | 4452 ± 1022 | 9266 ± 3384 | 17.8 ± 5.9 |
| Favorable† (n = 15) | 267 ± 108 | 7.3 ± 1.5 | 28.9 ± 8.3 | 5701 ± 2472 | 14,381 ± 2660 | 9.9 ± 1.6 |
| *P* value | $P < 0.05$ | $P = 0.057$ | $P = 0.155$ | $P = 0.561$ | $P = 0.155$ | $P = 0.388$ |

Values are expressed as mean ± standard error of the mean.
*Patients with a GOS score of 1, 2, or 3.
†Patients with a GOS score of 4 or 5.
*P* value obtained by Mann-Whitney *U* test for the difference between the two groups.

Only the CSF IL-1β concentration correlated with the CSF S100B concentration. However, we could not uncover the reason for this correlation. Further study is needed to clarify the precise relationship between CSF S100B and CSF IL-1β in severe TBI.

## REFERENCES


1. Zimmer DB, Cornwall EH, Landar A, Song W: The S100 protein family: history, function, and expression. *Brain Res Bull* 37:417–429, 1995.
2. Bianchi R, Garbuglia M, Verzini M, Giambanco I, Ivanenkov VV, Dimlich RV, Jamieson GA Jr, Donato R: S-100 (alpha and beta) binding peptide (TRTK-12) blocks S-100/GFAP interaction: identification of a putative S-100 target epitope within the head domain of GFAP. *Biochim Biophys Acta* 1313:258–267, 1996.
3. Biberthaler P, Mussack T, Wiedemann E, Gilg T, Soyka M, Koller G, Pfeifer KJ, Linsenmaier U, Mutschler W, Gippner-Steppert C, Jochum M: Elevated serum levels of S-100B reflect the extent of brain injury in alcohol intoxicated patients after mild head trauma. *Shock* 16:97–101, 2001.
4. Pelinka LE, Toegel E, Mauritz W, Redl H: Serum S 100 B: a marker of brain damage in traumatic brain injury with and without multiple trauma. *Shock* 19: 195–200, 2003.
5. Biberthaler P, Mussack T, Wiedemann E, Kanz KG, Koelsch M, Gippner-Steppert C, Jochum M: Evaluation of S-100b as a specific marker for neuronal damage due to minor head trauma. *World J Surg* 25:93–97, 2001.
6. Mussack T, Biberthaler P, Gippner-Steppert C, Kanz KG, Wiedemann E, Mutschler W, Jochum M: Early cellular brain damage and systemic inflammatory response after cardiopulmonary resuscitation or isolated severe head trauma: a comparative pilot study on common pathomechanisms. *Resuscitation* 49:193–199, 2001.
7. Pleines UE, Morganti-Kossmann MC, Rancan M, Joller H, Trentz O, Kossmann T: S-100 beta reflects the extent of injury and outcome, whereas neuronal specific enolase is a better indicator of neuroinflammation in patients with severe traumatic brain injury. *J Neurotrauma* 18:491–498, 2001.
8. Berger RP, Pierce MC, Wisniewski SR, Adelson PD, Clark RS, Ruppel RA, Kochanek PM: Neuron-specific enolase and S100B in cerebrospinal fluid after severe traumatic brain injury in infants and children. *Pediatrics* 109:E31, 2002.
9. Rothermundt M, Peters M, Prehn JH, Arolt V: S100B in brain damage and neurodegeneration. *Microsc Res Tech* 60:614–632, 2003.
10. Shohami E, Novikov M, Bass R, Yamin A, Gallily R: Closed head injury triggers early production of TNFα and IL-6 by brain tissue. *J Cereb Blood Flow Metab* 14:615–619, 1994.
11. Taupin V, Toulmond S, Serrano A, Benavides J, Zavala F: Increase in IL-6, IL-1 and TNF levels in rat brain following traumatic lesion. Influence of pre- and post-traumatic treatment with Ro5 4864, a peripheral-type (*p* site) benzodiazepine ligand. *J Neuroimmunol* 42:177–185, 1993.
12. Gaetani P, Tartara F, Pignatti P, Tancioni F, Rodriguez y Baena R, De Benedetti F: Cisternal CSF levels of cytokines after subarachnoid hemorrhage. *Neurol Res* 20:337–342, 1998.
13. Tarkowski E, Rosengren L, Blomstrand C, Wikkelso C, Jensen C, Ekholm S, Tarkowski A: Intrathecal release of pro- and anti-inflammatory cytokines during stroke. *Clin Exp Immunol* 110:492–499, 1997.
14. Otto L, Mcclain CJ, Gillespie M, Young B: Cytokines and metabolic dysfunction after severe head injury. *J Neurotrauma* 11:447–472, 1994.
15. Morganti-Kossmann MC, Rancan M, Otto VI, Stahel PF, Kossmann T: Role of cerebral inflammation after traumatic brain injury: a revisited concept. *Shock* 16:165–177, 2001.
16. Bell MJ, Kochanek PM, Doughty LA, Carcillo JA, Adelson PD, Clark RS, Wisniewski SR, Whalen MJ, DeKosky ST: Interleukin-6 and interleukin-10 in cerebrospinal fluid after severe traumatic brain injury in children. *J Neurotrauma.* 14:451–457, 1997.
17. Kossmann T, Hans V, Imhof HG, Trentz O, Morganti-Kossmann MC: Interleukin-6 released in human cerebrospinal fluid following traumatic brain injury may trigger nerve growth factor production in astrocytes. *Brain Res* 713:143–152, 1996.
18. Marion DW, Penrod LE, Kelsey SF, Obrist WD, Kochanek PM, Palmer AM, Wisniewski SR, DeKosky ST: Treatment of traumatic brain injury with moderate hypothermia. *N Engl J Med* 336:540–546, 1997.
19. Vos PE, Verbeek MM: Brain specific proteins in serum: Do they reliably reflect brain damage? *Shock* 18:481–482, 2002.
20. Csuka E, Morganti-Kossmann MC, Lenzlinger PM, Joller H, Trentz O, Kossmann T: IL-10 levels in cerebrospinal fluid and serum of patients with severe traumatic brain injury: relationship to IL-6, TNF-α, TGF-ββα1 and blood–brain barrier function. *J Neuroimmunol* 101:211–221, 1999.
21. Kossmann T, Stahel PF, Lenzlinger PM, Redl H, Dubs RW, Trentz O, Schlag G, Morganti-Kossmann MC: Interleukin-8 released into the cerebrospinal fluid after brain injury is associated with blood–brain barrier dysfunction and nerve growth factor production. *J Cereb Blood Flow Metab* 17:280–289, 1997.
22. Maier B, Schwerdtfeger K, Mautes A, Holanda M, Muller M, Steudel WI, Marzi I: Differential release of interleukins 6, 8, and 10 in cerebrospinal fluid and plasma after traumatic brain injury. *Shock* 15:421–426, 2001.
23. Teasdale G, Jennett B: Assessment of coma and impaired consciousness. A practical scale. *Lancet* 2:81–84, 1974.
24. Shiozaki T, Kato A, Taneda M, Hayakata T, Hashiguchi N, Tanaka H, Shimazu T, Sugimoto H: Little benefit from mild hypothermia therapy for severely head injured patients with low intracranial pressure. *J Neurosurg* 91:185–191, 1999.
25. Clatterbuck RE, Sipos EP: The efficient calculation of neurosurgically relevant volumes from computed tomographic scans using Cavalieri's Direct Estimator. *Neurosurgery* 40:339–342, 1997.
26. Jennett B, Bond M: Assessment of outcome after severe brain damage. A practical scale. *Lancet* 1:480–484, 1975.
27. Woertgen C, Rothoerl RD, Holzschuh M, Metz C, Brawanski A: Comparison of serial S-100 and NSE serum measurement after severe head injury. *Acta Neurochir (Wien)* 139:1161–1165, 1997.
28. Hardemark HG, Ericsson N, Kotwica Z, Rundstrom G, Mendel-Hartvig I, Olsson Y, Pahlman S, Persson L: S-100 protein and neuron-specific enolase in CSF after experimental traumatic or focal ischemic brain damage. *J Neurosurg* 71:727–731, 1989.
29. Woertgen C, Rothoerl RD, Metz C, Brawanski A: Comparison of clinical, radiologic, and serum marker as prognostic factors after severe head injury. *J Trauma* 47:1126–1130, 1999.
30. Raabe A, Grolms C, Keller M, Dohnert J, Sorge O, Seifert V: Correlation of computed tomography findings and serum brain damage markers following severe head injury. *Acta Neurochir (Wien)* 140:787–792, 1998.
31. Persson L, Hardemark H, Edner G, Ronne E, Mendel-Hartvig I: Pahlman S: S-100 protein in cerebrospinal fluid of patients with subarachnoid haemorrhage: a potential marker of brain damage. *Acta Neurochir (Wien)* 93:116–122, 1988.
32. Rossano F, Tufano R, Cipollaro de L'Ero G, Servillo G, Baroni A, Tufano MA, Servillo G, Baroni A, Tufano MA: Anesthetic agents induce human mononuclear leucocytes to release cytokines. *Immunopharmacol Immunotoxicol* 14:439–450, 1992.
33. Rickmann M, Wolff JR: Modifications of S100-protein immunoreactivity in rat brain induced by tissue preparation. *Histochem Cell Biol* 103:135–145, 1995.
34. Marshall LF, Marshall SB, Klauber MR, Clark MB: A new classification of head injury based on computerized tomography. *J Neurosurg* 75:S14–S20, 1991.

Annals of Nuclear Medicine Vol. 18, No. 1, 35–44, 2004

# PET measurements of CBF, OEF, and $CMRO_2$ without arterial sampling in hyperacute ischemic stroke: Method and error analysis

Masanobu IBARAKI,* Eku SHIMOSEGAWA,* Shuichi MIURA,* Kazuhiro TAKAHASHI,* Hiroshi ITO,* Iwao KANNO* and Jun HATAZAWA**

*Department of Radiology and Nuclear Medicine, Akita Research Institute, of Brain and Blood Vessels
**Division of Tracer Kinetics and Nuclear Medicine, Osaka University Graduate School of Medicine

A method for relative measurement of cerebral blood flow (CBF), oxygen extraction fraction (OEF), and metabolic rate of oxygen ($CMRO_2$) using positron emission tomography (PET) without arterial sampling in patients with hyperacute ischemic stroke was presented. ***Methods:*** The method requires two PET scans, one for $H_2{}^{15}O$ injection and one for ${}^{15}O_2$ inhalation, and calculates regional CBF, $CMRO_2$, and OEF relative to those at the reference brain region by means of table-lookup method. In this study, we calculated "relative lookup-tables" which relate relative CBF to relative $H_2{}^{15}O$ count, relative $CMRO_2$ to relative ${}^{15}O_2$ count, and relative OEF to relative ${}^{15}O_2/H_2{}^{15}O$ count. Two assumptions were applied to the lookup-table calculation: 1) In the reference region, CBF and OEF were assumed to be 50.0 ml/min/100 ml and 0.40, respectively, 2) Cerebral blood volume (CBV) was assumed to be constant at 4.0 ml/100 ml over the whole brain. Simulation studies were done to estimate the error of the present method derived from the assumptions. ***Results:*** For relative CBF measurements, 20% variation in reference CBF gave about ±10% error for measured relative CBF at maximum. Changes in CBV caused relatively large errors in measured OEF and $CMRO_2$ when relative CBF and OEF decreased. Errors for measured relative OEF caused by 50% variation in CBV were within ±8% at 0.8 of relative CBF and ±12% at 0.4 of relative CBF when relative OEF was greater than 1.0. ***Conclusion:*** CBV effects caused larger errors in estimated OEF and $CMRO_2$ in the region of the ischemic core with decreasing relative CBF and/or OEF but only slight errors in the region of "misery perfusion" with relative OEF values greater than 1.0. The present method makes PET measurements simpler than with the conventional method and increases understanding of the cerebral circulation and oxygen metabolism in patients with hyperacute stroke of several hours after onset.

**Key words:** PET, relative measurement, cerebral blood flow, oxygen metabolism, hyperacute stroke

## INTRODUCTION

EFFECTIVE TREATMENT for patients with hyperacute ischemic stroke requires urgent and accurate diagnosis of brain ischemia and ischemic injury in the emergency setting.[1,2] Measurement of cerebral blood flow (CBF) in the hyperacute stage of cerebral infarction with single photon emission computed tomography (SPECT) has been used to estimate the CBF threshold for subsequent infarction,[3] and to predict the probability of hemorrhagic complications after acute thrombolytic therapy.[4–6] Although these SPECT-CBF were normalized by reference CBF of the unaffected cerebral or cerebellar hemisphere instead of using absolute values, relative CBF threshold provided reliable signposts for the diagnosis and treatment of the hyperacute stage of cerebral infarction. In addition to CBF, measurements of brain metabolism are also strongly

Received May 29, 2003, revision accepted October 27, 2003.
For reprint contact: Masanobu Ibaraki, Ph.D., Department of Radiology and Nuclear Medicine, Akita Research Institute of Brain and Blood Vessels, 6–10 Senshu-Kubota Machi, Akita 010–0874, JAPAN.
E-mail: iba@akita-noken.go.jp

needed to provide more accurate information on the brain tissue and the applicability of therapy. Positron emission tomography (PET) has made possible the quantification of CBF, oxygen extraction fraction (OEF), and cerebral metabolic rate of oxygen ($CMRO_2$).[7-10] The OEF and $CMRO_2$ can indicate the area with a risk of evolving infarction. Although these metabolic-related images can be measured only by PET, the clinical use of PET study in the emergency setting is not feasible because of the relatively time-consuming method needed for quantification. Arterial cannulation for the blood sampling adds time and is sometimes impossible. Derdeyn et al. recently applied a count-based PET method to estimate OEF for prediction of ischemic stroke in patients with symptomatic carotid artery occlusion.[11,12] This method was first used by Jones et al.[13] and requires no arterial sampling. Although their studies showed a great prospect of clinical PET usage,[11,12] estimation of the methodological error has not been precisely evaluated so far.

We here propose a method for measurement of relative CBF, OEF, and $CMRO_2$ during hyperacute ischemic stroke. The method requires two PET scans without arterial sampling, one scan for $H_2{}^{15}O$ injection and the other for $^{15}O_2$ inhalation. Regional CBF, $CMRO_2$, and OEF are determined as relative to values in a reference brain region by means of a table-lookup procedure.[9,14] In this study, we calculated "relative lookup-tables" which relate relative CBF to relative $H_2{}^{15}O$ count, relative $CMRO_2$ to relative $^{15}O_2$ count, and relative OEF to relative $^{15}O_2/H_2{}^{15}O$ count. Two assumptions were applied to the lookup-table calculation: 1) In the reference brain region, CBF and OEF were assumed to be 50.0 m*l*/min/100 m*l* and 0.40, respectively, 2) Cerebral blood volume (CBV) was assumed to be constant at 4.0 m*l*/100 m*l* over the whole brain. Errors in relative CBF, OEF and $CMRO_2$ introduced by the assumptions were estimated by a simulation study.

To examine the applicability of the present method, we compared CBF, OEF, and $CMRO_2$ measured by the present method with quantitative values using arterial sampling data for 6 chronic stroke patients. We also presented relative CBF, OEF, and $CMRO_2$ images of a hyperacute stroke patient as an example of the application, which revealed a state of "misery-perfusion".

## MATERIALS AND METHODS

*Model*

Calculations of the PET count for the $H_2{}^{15}O$ injection were based on the single-compartment model for diffusible tracers originally developed by Kety.[15] Tissue concentration of $H_2{}^{15}O$, $C_t^{H_2O}(t)$, is described by the following equation.

$$C_t^{H_2O}(t) = fC_i(t) \otimes e^{-\frac{f}{p}t} \qquad \text{(Eq. 1)}$$

where $f$ is a CBF, $p$ is a partition coefficient of water in tissue to blood, and $C_i(t)$ is the arterial concentration of $H_2{}^{15}O$, which is usually measured by continuous arterial sampling for quantitative PET measurement. $\otimes$ denotes the convolution. $C_t^{H_2O}(t)$ and $C_i(t)$ are already corrected for radioactive decay. The PET count is given by integrating the tissue concentration over the scan time and is normalized to the PET count at the reference region to obtain the "relative $H_2{}^{15}O$ count," $R_{H_2O}$, as follows:

$$R_{H_2O} = \int_0^T C_t^{H_2O}(t)dt \Big/ \int_0^T C_{ref}^{H_2O}(t)dt \qquad \text{(Eq. 2)}$$

where $T$ is the scan time and $C_{ref}^{H_2O}(t)$ is the concentration of $H_2{}^{15}O$ at the reference region. In the present study, the ipsilateral cerebellum was chosen as the reference region. By assuming an absolute CBF value at the reference region, $R_{H_2O}$ can be calculated as a function of relative CBF normalized at the reference brain region, $R_{CBF}$. The calculated $R_{H_2O}$ is a table of the relative $H_2{}^{15}O$ count-relative CBF relation and is called "relative lookup-table" in this article. We can determine the relative CBF from the measured relative $H_2{}^{15}O$ count by using the relative lookup-table.

For $^{15}O_2$ inhalation, the model developed by Mintun et al.[10] for the measurement of OEF and $CMRO_2$ considers $^{15}O_2$ in the vascular space and metabolized $H_2{}^{15}O$, and gives the measured activity of $^{15}O$, $C_t^{O_2}(t)$, as

$$C_t^{O_2}(t) = EfC_i^O(t) \otimes e^{-\frac{f}{p}t} + VR(1 - 0.835E)C_i^O(t) + fC_i^W(t) \otimes e^{-\frac{f}{p}t} \qquad \text{(Eq. 3)}$$

where $C_i^O(t)$ and $C_i^W(t)$ are the arterial concentrations of $^{15}O_2$ and $H_2{}^{15}O$, respectively, $E$ is an OEF, $V$ is a CBV, and $R$ is a small-to large-vessel hematocrit ratio. $C_i^{O_2}(t)$ consists of three components: activity of $H_2{}^{15}O$ metabolism created locally from $^{15}O_2$ extracted to the tissue, activity of unextracted $^{15}O$ in the vascular spaces, and activity of $H_2{}^{15}O$ by arterial recirculation of $H_2{}^{15}O$ from all tissues. The $CMRO_2$ is related to the CBF and OEF as

$$CMRO_2 = OEF \cdot CBF \cdot [O_2] \qquad \text{(Eq. 4)}$$

where $[O_2]$ is the total oxygen content of arterial blood. The PET count is given by integrating the tissue concentration over the scan time and is normalized to the PET count at the reference brain region to obtain the "relative $^{15}O_2$ count," $R_{O_2}$, as follows:

$$R_{O_2} = \int_0^T C_t^{O_2}(t)dt \Big/ \int_0^T C_{ref}^{O_2}(t)dt \qquad \text{(Eq. 5)}$$

where $C_{ref}^{O_2}(t)$ is the activity in the reference region. By assuming absolute CBF and OEF values at the reference region, $R_{O_2}$ can be calculated as a function of relative $CMRO_2$ normalized at the reference region, $R_{CMRO_2}$. As known by Eq. 4, $R_{O_2}$ is also a function of relative CBF and OEF. In the calculation of $R_{O_2}$, CBV is assumed to be constant over the whole brain. As with $CMRO_2$, "relative $^{15}O_2/H_2{}^{15}O$ count," $R_{O_2/H_2O}$, is calculated as a function

of relative OEF, $R_{OEF}$. By applying calculated $R_{O_2}$ and $R_{O_2/H_2O}$ called "relative lookup-table," we can determine the relative $CMRO_2$ and OEF from the measured relative $^{15}O_2$ and $^{15}O_2/H_2{}^{15}O$ counts, respectively.

*Simulation Study*

We performed the calculation of the relative lookup-table and the simulation study to estimate the errors of the present method. We used Eq. 1 and Eq. 3 to calculate the activity curve as a function of the time after tracer supply for various CBF and OEF. The results were integrated over the scan duration, 180 second for both Eq. 2 and Eq. 5, then converted to the relative lookup-table. $p$ was fixed at 0.8 ml/ml in all calculations. The parameters for calculations in the reference region were fixed at 50.0 ml/min/100 ml for CBF and 0.40 for OEF. CBV was assumed to be constant at 4.0 ml/100 ml over the whole brain. The arterial activity curves used in the present calculations are shown in Figure 1. The curves for $H_2{}^{15}O$ injection and $^{15}O_2$ inhalation were described by the functions, $t\exp(-t/89.3)$ and $t^2\exp(-(t/50.7)^{1.5}) + 22.8t^{0.5}$, respectively, which reproduced well the typical arterial activity

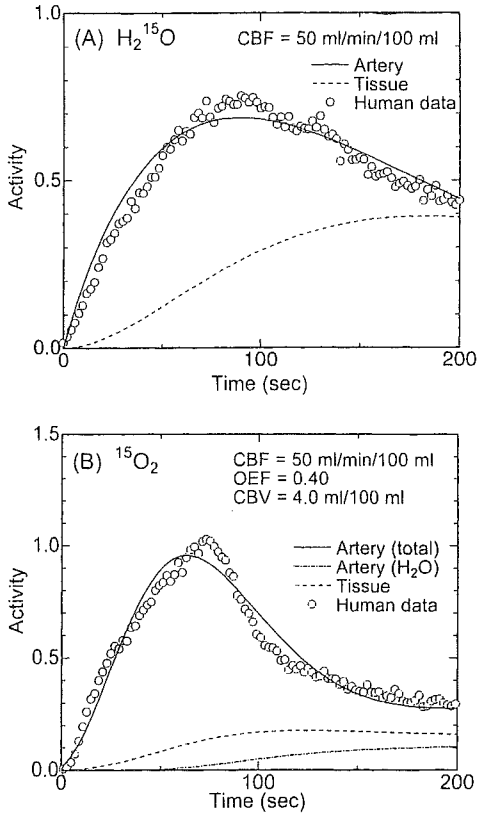


**Fig. 1** The arterial activity curve used in simulations and the calculated tissue activity curve for 120 sec slow infusion of $H_2{}^{15}O$ (A) and 90 sec inhalation of $^{15}O_2$ (B) are shown. The actual human data as an example are also shown. The tissue activity was calculated under the conditions of 50.0 ml/min/100 ml for CBF, 0.40 for OEF, and 4.0 ml/100 ml for CBV. To calculate $^{15}O_2$ activity, we need the fractions of $^{15}O_2$ and $H_2{}^{15}O$ to total arterial activity; therefore, the $H_2{}^{15}O$ fraction from recirculation is also shown. The tissue activity curves were integrated from 0 s to 180 s to calculate the PET count.

**Table 1** Patient information

| Pat. | year/sex | vascular lesion | after onset |
|---|---|---|---|
| 1 | 75/F | Lt. IC stenosis (>95%) | 1 month |
| 2 | 52/M | Lt. IC occlusion | 6 months |
| 3 | 71/F | Rt. IC stenosis (>90%) | asymptomatic |
| 4 | 67/M | Lt. MCA stenosis | 1 month |
| 5 | 62/M | Rt. IC stenosis | 1 month |
| 6 | 70/M | Rt. IC stenosis (>80%) | 3 months |

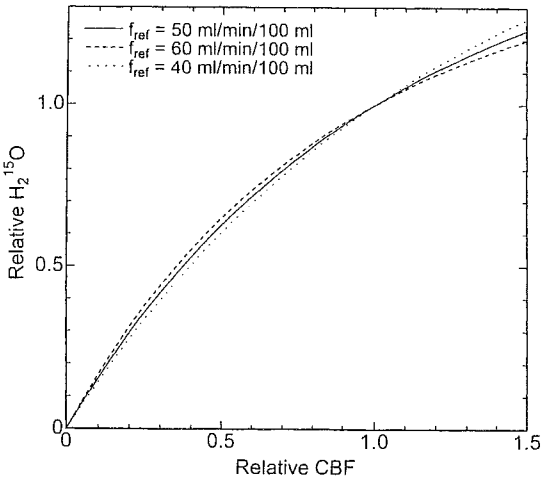


**Fig. 2** Calculated relative $H_2{}^{15}O$ PET count as a function of relative CBF. Both PET count and CBF were relative values to the reference, and the reference CBF ($f_{ref}$) was assumed to be 50.0 ml/min/100 ml. Calculated results with reference CBF values of 40.0 and 60.0 ml/min/100 ml are also shown.

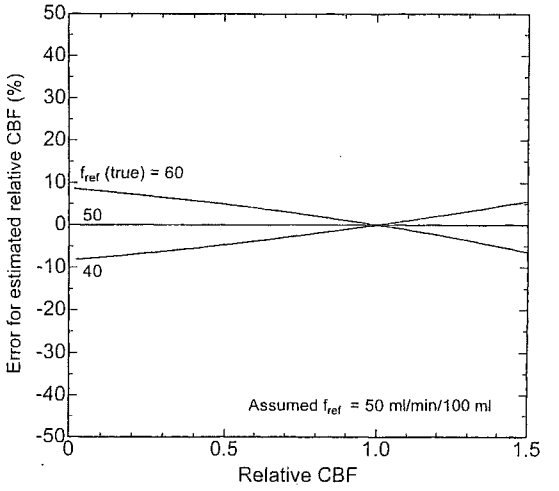


**Fig. 3** Errors in the measured relative CBF by the table-lookup procedure where the reference CBF ($f_{ref}$) was assumed to be 50.0 ml/min/100 ml but the actual CBF ($f_{ref}$ (true)) was 40.0 or 60.0 ml/min/100 ml.

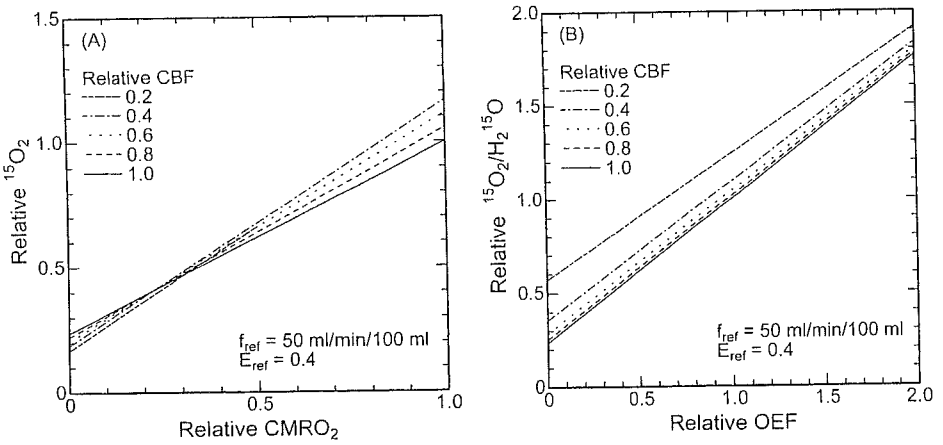


**Fig. 4** Calculated relative $^{15}O_2$ (A) and $^{15}O_2/H_2{}^{15}O$ (B) PET counts as a function of relative $CMRO_2$ and OEF, respectively. For the reference region, 50.0 ml//min/100 ml CBF ($f_{ref}$), 0.40 OEF ($E_{ref}$), and 4.0 ml//100 ml CBV were assumed. The whole-brain CBV was assumed to be 4.0 ml//100 ml, the same as the reference region. The results for the relative CBF from 0.2 to 1.0 were presented.

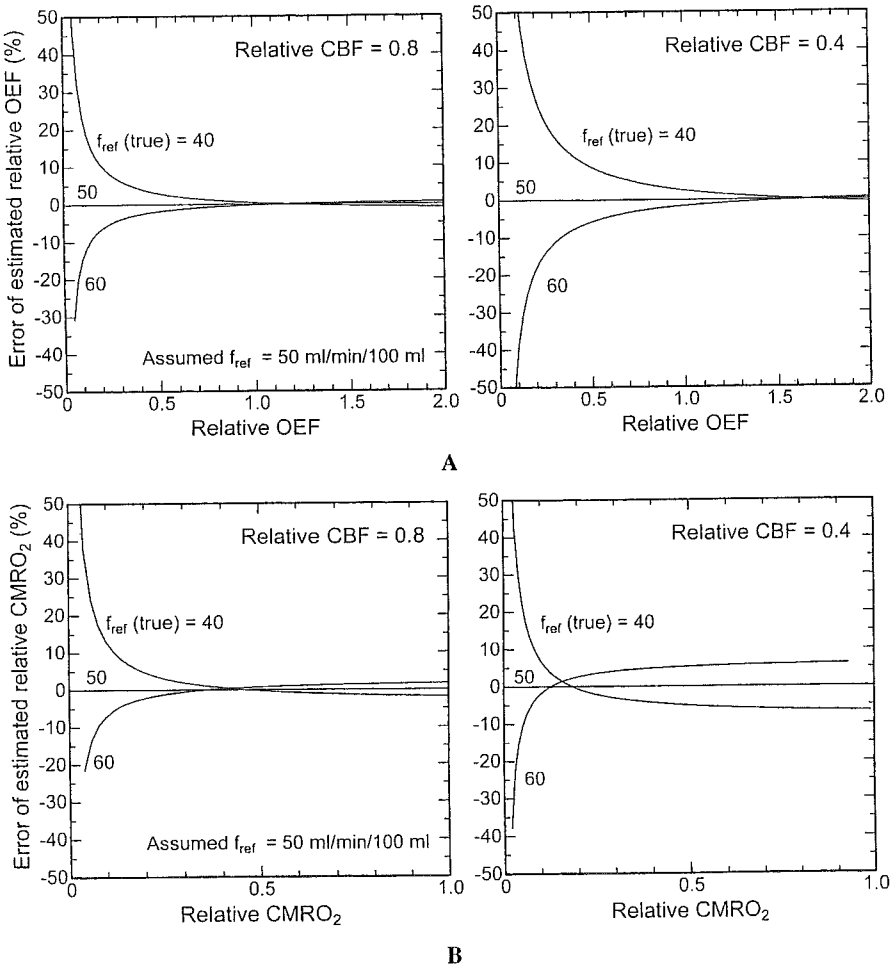


**Fig. 5** Errors in measured relative OEF (A) and $CMRO_2$ (B) where the reference CBF ($f_{ref}$) was assumed to be 50.0 ml//min/100 ml but the actual CBF ($f_{ref}$ (true)) was 40.0 or 60.0 ml/min/100 ml, which correspond to ±20% variations of the reference CBF. Errors are shown for two cases, when relative CBF was 0.8 (low-grade ischemia) and 0.4 (high-grade ischemia), respectively.

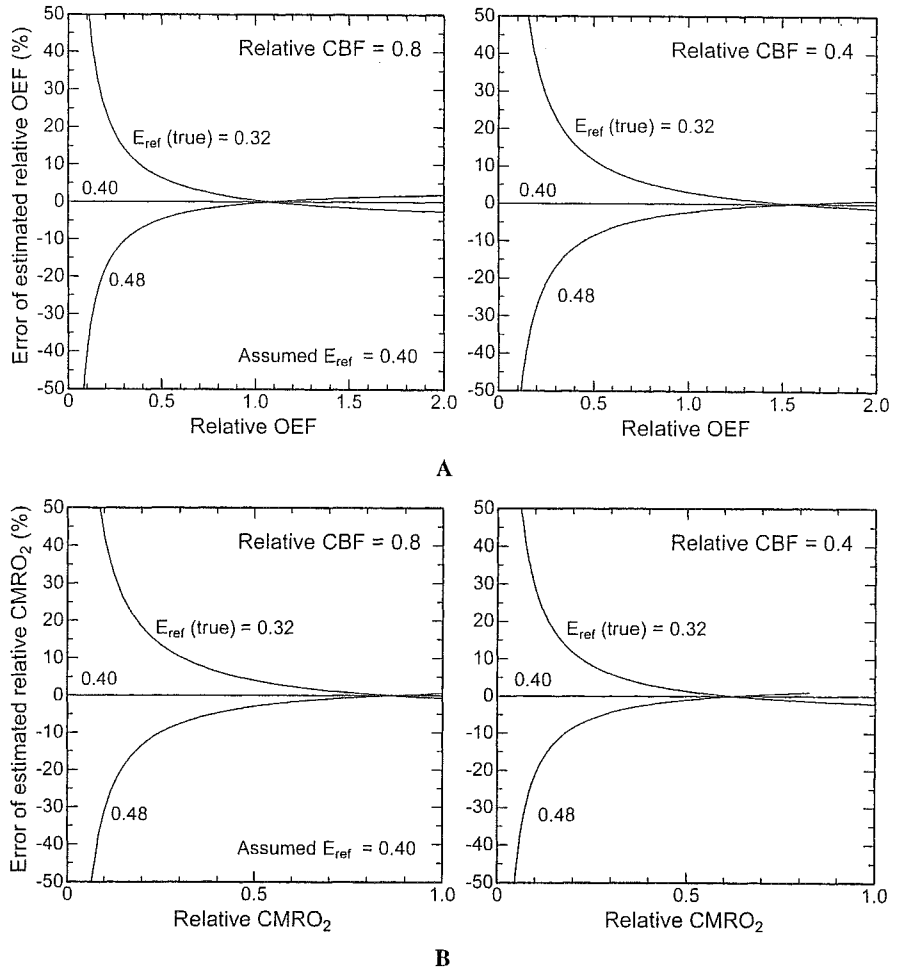


**Fig. 6** Errors in measured relative OEF (A) and $CMRO_2$ (B) where the reference OEF ($E_{ref}$) was assumed to be 0.40 but the actual OEF ($E_{ref}$ (true)) was 0.32 or 0.48, which correspond to ±20% variations of the reference OEF.

measured at our institute after slow infusion of $H_2{}^{15}O$ for 120 second and continuous inhalation of $^{15}O_2$ for 90 second. Figure 1 also show actual human data as an example. For $^{15}O_2$ calculations, arterial concentrations of $^{15}O_2$ and $H_2{}^{15}O$, $C_i^O(t)$ and $C_i^W(t)$ in Eq. 3, are required rather than total arterial activity. The fractions of $C_i^O(t)$ and $C_i^W(t)$ relative to the total activity were estimated according to the method of Iida et al.[16]

We next performed calculations to estimate the effects of errors in the reference parameters. The calculations were done with reference CBF values between 40.0 and 60.0 m*l*/min/100 m*l* and reference OEF values between 0.32 and 0.48, which correspond to 20% error in the assumed values. Although CBV was fixed at 4.0 m*l*/100 m*l* in the above calculations, we did other calculations in which the CBV varied between 2.0 and 6.0 m*l*/100 m*l* to estimate errors introduced by assuming a constant CBV.

*Patient Study*

To examine the differences between relative values by the present method and quantitative values, we performed a PET study with arterial blood sampling for 6 unilateral stroke patients in the chronic stage. The measurements were performed with a Headtome-V PET scanner,[17] and the PET procedures were the same as in the previous studies.[18,19] The patient information was summarized in Table 1. We computed two image sets for each patient, relative CBF, OEF, and $CMRO_2$ images by the present method, and absolute images by the conventional method using the blood data. CBV effects for quantitative OEF and $CMRO_2$ were corrected by PET measurements with C $^{15}O$ inhalation.[10,22] For relative CBF, OEF, and $CMRO_2$ images, ipsilateral cerebellum was chosen as the reference region. For region of interest (ROI) analysis to calculate lesion-contralateral hemisphere ratio of CBF, OEF, and $CMRO_2$, we picked one hypo-perfused slice for each patient. The circular ROIs with 16 mm diameter covered the cerebral cortex of the lesion and contralateral hemisphere, and lesion-contralateral ratios were calculated for each patient and each image.

We also performed PET measurement without blood sampling for a patient (67-year-old female, 4 hours after

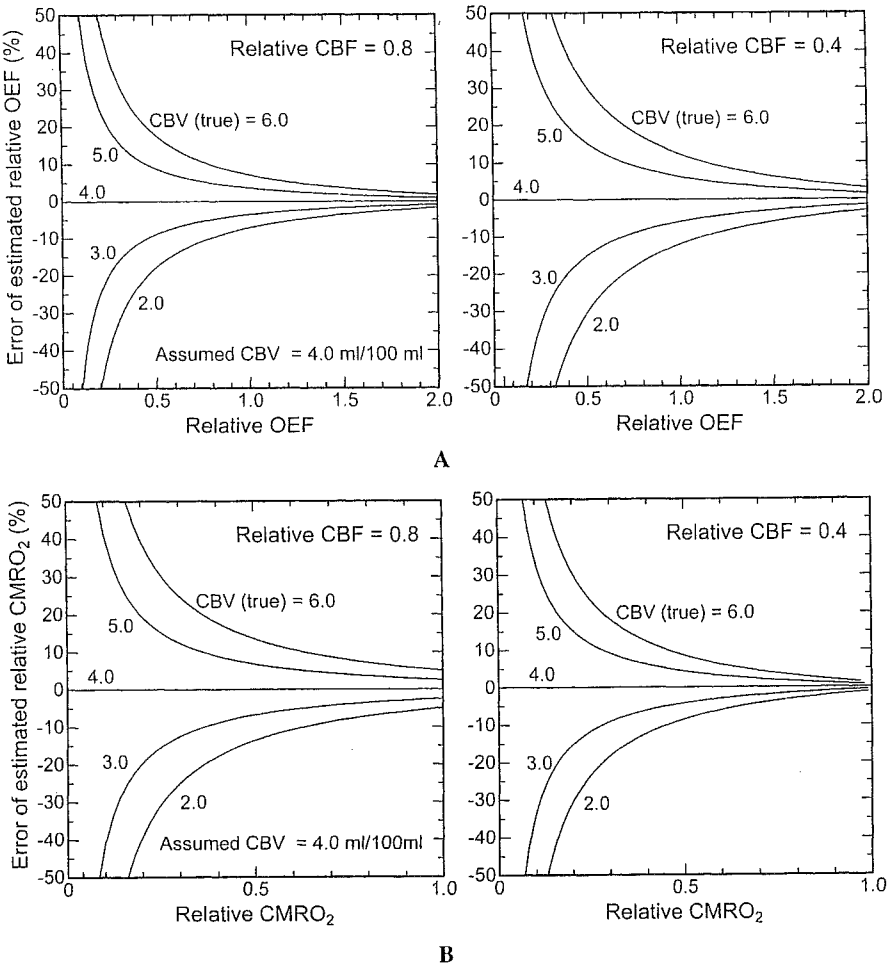


**Fig. 7** Errors in measured relative OEF (A) and $CMRO_2$ (B) caused by CBV variation. The CBV was between 2.0 and 6.0 m*l*/100 m*l*, but the reference CBV was fixed at 4.0 m*l*/100 m*l*.

onset of MCA occlusion), as an example of the application for hyperacute stroke.

## RESULT

*Relative CBF*

A calculated relative lookup-table which relates the relative $H_2{}^{15}O$ PET count ($R_{H_2O}$) to relative CBF ($R_{CBF}$) is shown in Figure 2. The reference CBF was assumed to be 50.0 m*l*/min/100 m*l*. From the relative lookup-table and the measured relative PET count, we can determine relative CBF by means of the table-lookup procedure. For example, if the relative PET count was 0.53, we can determine relative CBF to be 0.40. The lookup-tables for 40.0 and 60.0 m*l*/min/100 m*l* of the reference CBF are also shown in Figure 2. The errors in measured relative CBF resulting from the table-lookup method (reference CBF was assumed to be 50.0 m*l*/min/100 m*l*) for each case where the true reference CBF was 40.0, 50.0, or 60.0 m*l*/min/100 m*l* are shown in Figure 3. A discrepancy between the assumed and true reference CBF caused an error in the measured relative CBF, but there was no error if the assumed reference CBF was equal to the true reference CBF. For reference CBF variations between 40.0 and 60.0 m*l*/min/100 m*l*, the error was less than ±10%.

*Relative $CMRO_2$ and OEF*

A calculated relative lookup-table which relates the relative $^{15}O_2$ PET count ($R_{O_2}$) to relative $CMRO_2$ ($R_{CMRO_2}$) is shown in Figure 4 (*left panel*). The reference CBF and OEF values were assumed to be 50.0 m*l*/min/100 m*l* and 0.40, respectively. CBV in the whole brain was assumed to be 4.0 m*l*/100 m*l*. Because the relative $^{15}O_2$ PET count depends not only on the relative $CMRO_2$ but also on the relative CBF, the results for various relative CBF values, 1.0, 0.8, 0.6, 0.4, and 0.2, are shown. A calculated relative lookup-table which relates the relative $^{15}O_2/H_2{}^{15}O$ PET count ($R_{O_2/H_2O}$) to relative OEF ($R_{OEF}$) is shown in Figure 4 (*right panel*). The reference CBF and OEF were the same as those in the $^{15}O_2$ PET count calculations. As with relative CBF, lookup-table and measured relative PET counts allow for the determination of relative $CMRO_2$

**Table 2** Lesion-contralateral ratios of CBF, OEF and $CMRO_2$ by two methods, and the ratio of the present method (relative method) to quantitative method (absolute method)

| Pat. | Quantitative PET | | | Relative PET | | | Rel./Quant. | | |
|---|---|---|---|---|---|---|---|---|---|
| | CBF | OEF | $CMRO_2$ | CBF | OEF | $CMRO_2$ | CBF | OEF | $CMRO_2$ |
| 1 | 0.884 | 1.030 | 0.911 | 0.896 | 1.035 | 0.928 | 1.013 | 1.005 | 1.019 |
| 2 | 0.830 | 1.073 | 0.886 | 0.844 | 1.073 | 0.902 | 1.018 | 1.000 | 1.018 |
| 3 | 0.956 | 1.106 | 1.058 | 0.959 | 1.129 | 1.082 | 1.003 | 1.021 | 1.023 |
| 4 | 0.831 | 0.905 | 0.749 | 0.833 | 0.901 | 0.746 | 1.002 | 0.995 | 0.996 |
| 5 | 0.797 | 1.195 | 0.944 | 0.799 | 1.208 | 0.957 | 1.002 | 1.011 | 1.014 |
| 6 | 0.800 | 1.044 | 0.836 | 0.800 | 1.042 | 0.836 | 1.001 | 0.998 | 1.000 |

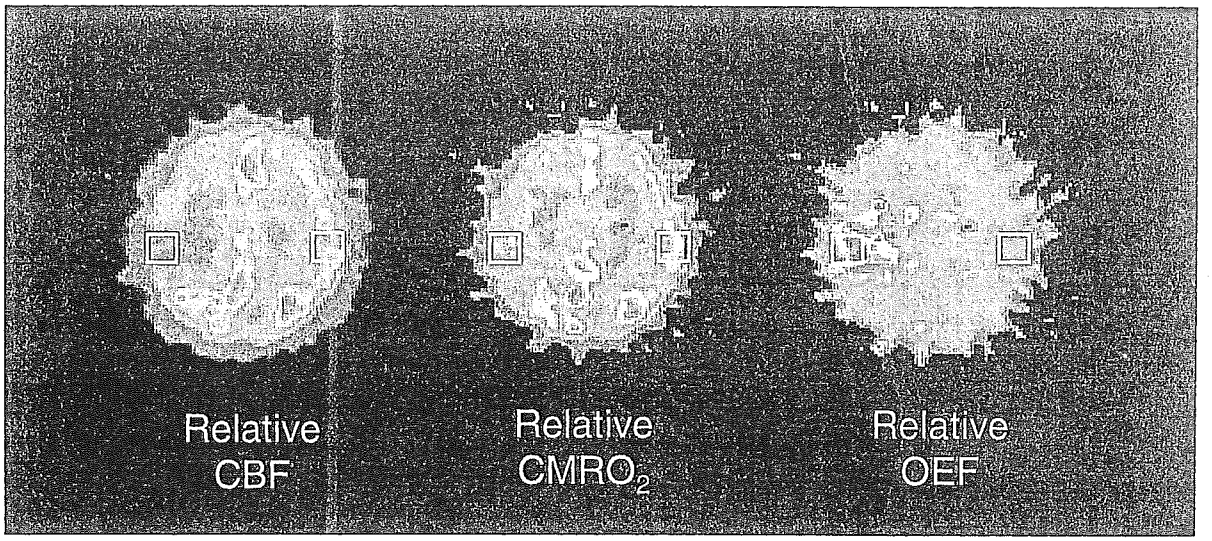


**Fig. 8** Images of relative CBF (*left*), $CMRO_2$ (*center*), and OEF (*right*) from a 67-year-old woman with right middle cerebral artery occlusion. PET measurements after $H_2{}^{15}O$ injection and $^{15}O_2$ inhalation were made 4 hours after onset. Application of region of interest (ROI) markers on the lesion and the contralateral brain region is shown. Ratios of lesion to contralateral CBF, $CMRO_2$, and OEF were 0.45, 0.71 and 1.60, respectively.

and OEF. The errors of measured relative OEF (A) and $CMRO_2$ (B) where the true reference CBF was 40.0, 50.0, or 60.0 m*l*/min/100 m*l* but was assumed to be 50.0 m*l*/min/100 m*l* are shown in Figure 5. CBF of 40.0 and 60.0 m*l*/min/100 m*l* correspond to ±20% error of the assumed reference CBF (50.0 m*l*/min/100 m*l*). In Figure 5, the errors for two cases in which relative CBF was 0.8 and 0.4 corresponding to low- and high-grade ischemia, respectively, are shown. The errors of measured relative OEF caused by the inadequate assumption of the reference CBF with 20% error were smaller than 3% at relative OEF greater than 1.0 but were larger at low relative OEF values. The errors of measured relative $CMRO_2$ showed the same trends as those of relative OEF but were about ±6% at relative $CMRO_2$ values greater than 0.5 for high-grade ischemia. The errors of measured relative OEF (A) and $CMRO_2$ (B) for each case in which the true reference OEF is 0.32, 0.40, or 0.48, but is assumed to be 0.40, are shown in Figure 6. The errors of measured relative OEF and $CMRO_2$ caused by the inadequate assumption of the reference OEF with 20% error were similar and were smaller than 5% at relative OEF values greater than 1.0 and at relative $CMRO_2$ values greater than 0.5.

CBV effects on measurement of relative OEF (A) and $CMRO_2$ (B) are shown in Figure 7. The CBV varied between 2.0 and 6.0 m*l*/100 m*l* which correspond to ±50% of 4.0 m*l*/100 m*l*, but the reference CBV was fixed at 4.0 m*l*/100 m*l*. The errors of measured relative OEF increased as relative OEF and relative CBF decreased. At high OEF values (relative OEF > 1.0), relative OEF errors were less than ±8% at 0.8 of relative CBF and ±12% at 0.4 of relative CBF. In calculation of the $CMRO_2$, the magnitude of error was at the same level as that of relative OEF, but decreased as relative CBF decreased.

*Patient Study*

Lesion-contralateral ratios of CBF, OEF and $CMRO_2$ by two methods for 6 unilateral stroke patients in the chronic stage were summarized in Table 2. The ratio of the present method (relative method) to quantitative method

(absolute method) was also shown. The maximum difference between the two methods, 1.023, appeared in $CMRO_2$ for patient 3.

Relative CBF, $CMRO_2$, and OEF images from a 67-year-old woman with right middle cerebral artery occlusion representative of application of the present method to hyperacute stroke are shown in Figure 8. PET measurements after $H_2{}^{15}O$ injection and $^{15}O_2$ inhalation were performed 4 hours after stroke onset with a Headtome-V scanner (Shimadzu Corp., Kyoto, Japan).[17] Total measurement time including preparation and transmission scanning for attenuation correction was 30 min. Relative CBF, $CMRO_2$, and OEF in each pixel were calculated by means of the relative table-lookup method. Application of the region of interest (ROI) on the lesion and contralateral brain region is shown (Fig. 8). CBF, $CMRO_2$, and OEF values relative to the reference brain region (cerebellum) were 0.33/0.73 (lesion/contralateral side), 0.59/0.83, and 1.81/1.13, respectively. Therefore, ratios for the lesion to the contralateral side for relative CBF, $CMRO_2$, and OEF were 0.45, 0.71, and 1.60, respectively. These values indicated a state of "misery-perfusion" with CBF decreased and OEF increased to maintain the $CMRO_2$.[20]

## DISCUSSION

Quantitative PET measurement of brain circulation and metabolism needs some complicated procedures, and takes more than 1 hour even for the basic examination to obtain the data of CBF, $CMRO_2$, and OEF. Arterial cannulation into the radial artery for input function measurement is the most time-consuming and invasive process, and it lengthens the total examination time of PET study. Especially in the emergency setting, examination for diagnostic imaging should be sufficiently shortened to decide the appropriate therapeutic strategy with minimization of painful procedures. We presented a method of relative PET measurement for cerebral circulation and oxygen metabolism during hyperacute stroke. Because this method is based on measurements of relative PET counts, we need only two emission scans after $H_2{}^{15}O$ injection and $^{15}O_2$ inhalation; blood samples are not needed. This makes the PET measurements simpler than the conventional quantitative measurements, shortens the scan time, and is suitable in the emergency setting for patients with hyperacute stroke. We estimated that a total measurement time of only about 30 min or less including preparation and transmission scanning would be needed. The present method provides information on "misery-perfusion" indicated by an increased OEF of the ischemic brain region, which can be measured only by PET.

In the present method, we can determine the relative CBF from the measured relative $H_2{}^{15}O$ PET count by using calculated relative lookup-table. Relative $^{15}O_2$ PET counts depend not only on relative $CMRO_2$ but also on relative CBF and OEF because $^{15}O_2$ PET count is a linear function of OEF and a nonlinear function of CBF (Eq. 3). This means that the relative $CMRO_2$ can not be determined from the relative $^{15}O_2$ PET count alone: both the relative $^{15}O_2$ and $H_2{}^{15}O$ PET counts are required. For example, when the relative $H_2{}^{15}O$ PET count of 0.53 corresponding to 0.40 for relative CBF and the relative $^{15}O_2$ PET count of 0.77 are measured, we can determine the relative $CMRO_2$ as 0.60 and the relative OEF as 1.50 by using relative lookup-table for 0.40 of relative CBF. By applying these procedures to $H_2{}^{15}O$ and $^{15}O_2$ images pixel by pixel, we can obtain relative CBF, OEF, and $CMRO_2$ images. Derdeyn et al. applied relative OEF measurements in patients with symptomatic carotid artery occlusion and looked on the relative $^{15}O_2/H_2{}^{15}O$ PET count as the relative OEF predicting the risk of stroke.[11,12] As seen in Figure 4 (*right panel*), however, there is not a one-to-one correspondence between relative $^{15}O_2/H_2{}^{15}O$ PET count and relative OEF. For example, a relative $^{15}O_2/H_2{}^{15}O$ PET count of 1.0 corresponds to a relative OEF of between 0.63 and 1.0, depending on the relative CBF. Thus, we should estimate relative OEF from the measured relative $^{15}O_2/H_2{}^{15}O$ PET count with consideration of relative CBF.

We examined the differences between the present method and conventional quantitative method for lesion-contralateral ratios of CBF, OEF, and $CMRO_2$ for chronic stroke patients. The difference between the present method (relative method) and quantitative method (absolute method) were relatively small as shown in Table 2, and within the valuation by the simulations. The maximum difference between the two methods, 1.023 of $CMRO_2$ for patient 3, was due to CBV effect. Lesion-contralateral ratio of CBV for patient 3 measured by $C^{15}O$ inhalation was about 1.2 and the highest among the patients, although these data are not shown in this article. CBF decreases in the patients were relatively mild (0.797–0.956), and therefore further study of a large number of patients with various CBF would be desirable to validate the applicability in various types of patients.

Simulations resulted in different curves depending on the value of the assumed reference CBF (Fig. 2). This was caused by the nonlinear relation between PET count and CBF. The reference CBF variation between 40.0 and 60.0 m*l*/min/100 m*l*, corresponding to ±20% variation from 50.0 m*l*/min/100 m*l*, introduced a maximum ±10% error in the measured relative CBF at its low range; larger variations will cause larger errors. In other words, we can determine the relative CBF with a less than ±10% error if variation in the reference CBF remains less than ±20%. This suggests that care must be taken when selecting the reference region. An unaffected region, such as the ipsilateral cerebellum, must be chosen to reduce errors in measured CBF.

The calculation results showed the existence of $^{15}O_2$ PET counts even if OEF equals 0. This was caused by $^{15}O_2$ activity being distributed in the vascular space that was

not extracted into the tissue space and $H_2{}^{15}O$ activity by recirculation water. This offset effect emphasized the error at low OEF and $CMRO_2$ values, but the errors rapidly decreased at higher values (Figs. 5, 6). If the main interest of the study is the detection of "misery-perfusion" in which the OEF increases to maintain $CMRO_2$ as CBF decreases, the simulations yielded positive results because the errors caused by variation of assumed CBF and OEF reference values were relatively small at high range, less than 6% at relative OEF values greater than 1.0 and relative $CMRO_2$ values greater than 0.5.

Because the present method applies only two PET scans, we can not obtain CBV which can be measured quantitatively by $C^{15}O$ inhalation.[21] In quantitative oxygen metabolism measurements, CBV is known to be one of the major error sources.[22–24] For the calculation of the relative lookup-table, we assumed a constant CBV value in whole brain. This results in identical CBV values for both the normal and affected brain region, possibly causing significant errors of measured relative $CMRO_2$ and OEF. The degree of the CBV variation in the brain of the acute stroke patient is still controversial. Powers et al. performed PET study for 7 patients with unilateral carotid artery occlusion and CBF reductions in ischemic but uninfarcted regions of brain. They reported increased CBV in regions with decreased CBF, with the CBV ratio of symptomatic to asymptomatic hemisphere of the 7 patients varying between 1.0 and 1.5.[25] Hatazawa et al. reported CBV measurement by dynamic susceptibility contrast-enhanced MRI for 9 patients with unilateral occlusion of either the middle cerebral artery or internal carotid artery within 6 hours after onset.[26] In the brain regions with mild (relative CBF > 0.60) and moderate (0.40 < relative CBF < 0.60) hypoperfusion, the mean relative CBV values were $1.29 \pm 0.31$ and $0.94 \pm 0.49$, respectively. Derdeyn et al. investigated the relationship between CBV and OEF in a large sample of patients with unilateral carotid artery occlusion enrolled in a prospective study of hemodynamic factors and stroke risk.[27] They showed that the ipsilateral-to-contralateral CBV ratio varied between 0.7 and 1.5. Based on these data, the present simulations showed the effect of CBV errors, 50% variation at 4.0 m*l*/100 m*l*. When measuring relative OEF and $CMRO_2$, lower relative CBF and OEF values will introduce larger errors. A reduction in CBF and OEF increases the ratio of the residual $^{15}O_2$ in the vascular space to that extracted into the tissue and emphasizes the CBV effects. For example, when detecting "misery-perfusion," the measured OEF errors introduced by CBV effects are less than ±8% for low-grade ischemia (0.8 of relative CBF) and ±12% for high-grade ischemia (0.4 of relative CBF). Again, we emphasize that CBV effect must be considered for the change of relative OEF in the ischemic core, whereas relative OEF in the remediable area for hyperacute thrombolytic therapy would be subject to less error by CBV effect.

## CONCLUSION

We presented a method for PET measurement of relative CBF, OEF and, $CMRO_2$ with $H_2{}^{15}O$ injection and $^{15}O_2$ inhalation. The method is feasible to apply in patients with the hyperacute stage of cerebral infarction without the need for arterial sampling. In the present method, relative CBF, OEF, and $CMRO_2$ are determined by the table-lookup procedure. For the calculation of the relative lookup-table, CBF and OEF in the reference brain region were assumed to be 50.0 m*l*/min/100 m*l* and 0.40, respectively. Cerebral blood volume (CBV) was assumed to be constant at 4.0 m*l*/100 m*l* over the whole brain. For relative CBF calculation, the present simulation study revealed that 20% variation of the reference CBF value resulted in a maximum error of about 10%. CBV effects caused larger errors in measured OEF and $CMRO_2$ when CBF and/or OEF were severely decreased, mandating caution when analyzing the heavily damaged ischemic core. Sequential measurements of cerebral circulation and oxygen metabolism by the present method within a sufficiently short examination time would easily demonstrate the present salvageable area in an emergency and would have the possibility to provide useful information for application of thrombolytic or neuroprotective therapy in patients with hyperacute stroke.

## REFERENCES


1. The National Institute of Neurological Disorders and Stroke rt-PA Stroke Study Group. Tissue plasminogen activator for acute ischemic stroke. *N Eng J Med* 1995; 333: 1581–1587.
2. Hacke W, Kaste M, Fieschi C, Toni D, Lesaffre E, von Kummer R, et al. Intravenous thrombolysis with recombinant tissue plasminogen activator for acute hemispheric stroke. The European Cooperative Acute Stroke Study (ECASS). *JAMA* 1995; 274: 1017–1025.
3. Shimosegawa E, Hatazawa J, Inugami A, Fujita H, Ogawa T, Aizawa Y, et al. Cerebral infarction within six hours of onset: prediction of completed infarction with technetium-99m-HMPAO SPECT. *J Nucl Med* 1994; 35: 1097–1103.
4. Ueda T, Hatakeyama T, Kumon Y, Sasaki S, Uraoka T. Evaluation of risk of hemorrhagic transformation in local intra-arterial thrombolysis in acute ischemic stroke by initial SPECT. *Stroke* 1994; 25: 298–203.
5. Ezura M, Takahashi A, Yoshimoto T. Evaluation of regional cerebral blood flow using single photon emission tomography for the selection of patients for local fibrinolytic therapy of acute cerebral embolism. *Neurosurg Rev* 1996; 19: 231–236.
6. Ueda T, Sakaki S, Yuh WT, Nochide I, Ohta S. Outcome in acute stroke with successful intra-arterial thrombolysis and predictive value of initial single-photon emission-computed tomography. *J Cereb Blood Flow Metab* 1999; 19: 99–108.
7. Frackowiak RS, Lenzi GL, Jones T, Heather JD. Quantitative measurement of regional cerebral blood flow and

JOURNAL OF NEUROTRAUMA
Volume 21, Number 7, 2004

Pp. 923–931

# Src Family Kinase Inhibitor PP1 Reduces Secondary Damage after Spinal Cord Compression in Rats

CHIHIRO AKIYAMA,[1] TAKAMICHI YUGUCHI,[2] MASAMI NISHIO,[1] TAKAHIRO TOMISHIMA,[1] TOSHIYUKI FUJINAKA,[1] MASAAKI TANIGUCHI,[1] YOSHIKAZU NAKAJIMA,[1] EIJI KOHMURA,[3] and TOSHIKI YOSHIMINE[1]

## ABSTRACT

**The synthetic pyrazolopyrimidine, 4-amino-5-(4-methylphenyl)-7-(t-butyl)pyrazolo[3,4-d]pyrimidine (PP1) is a novel, potent, and selective inhibitor of Src family tyrosine kinases. Vascular permeability appears to be mediated by vascular endothelial growth factor (VEGF), which requires the activation of downstream Src family kinases to exert its function. This study investigates the effects of PP1 on vascular permeability and inflammatory response in a rat spinal cord compression model. Ten minutes after compression, PP1 (PP1 group) or the vehicle only (control group) was administered. On days 1, 3, and 7 after compression, the spinal cords were removed and examined histopathologically to determine the expression of VEGF and the extent of edema and inflammation. The dry-weight method was used to measure the water content of the spinal cords. The mRNA levels of tumor necrosis factor a (TNF$\alpha$) and interleukin 1$\beta$ (IL-1$\beta$), which is related to inflammatory responses, were measured with a real-time polymerase chain reaction (RT-PCR) system 6 h after compression. Although VEGF expression was similar in both groups, the extent of contusional lesion in the PP1 group was reduced by approximately 35% on day 3. Moreover, the water content on days 1, 3, and 7 was significantly reduced and macrophage infiltration on days 3 and 7 was dramatically reduced in the PP1 group. TNF$\alpha$ and IL-1$\beta$ mRNA expression in the PP1 group were also significantly reduced. These results indicate that PP1 reduces secondary damage after spinal cord injury.**

**Key words:** edema; macrophage infiltration; PP1; secondary damage; spinal cord injury; Src family kinase inhibitor

## INTRODUCTION

FOLLOWING SPINAL CORD INJURY, vascular permeability increases around the area of the injury, which may lead to both edema formation and inflammation eventually progressing to secondary tissue damage (Orlicek et al., 1999; Earnhardt et al., 2002). Controlling vascular permeability and inflammatory responses therefore, may be important for the attenuation of secondary damage. Vascular endothelial growth factor (VEGF) is involved in the aggravation of secondary damage after spinal cord injury (Sköld et al., 2000). VEGF is a well-known spe-

[1]Department of Neurosurgery, Osaka University Medical School, Suita, Japan.
[2]Department of Neurosurgery, Spine and Spinal Cord Center, Yukioka Hospital, Osaka, Japan.
[3]Department of Neurosurgery, Kobe University Graduate School of Medicine, Kobe, Japan.

cific endothelial mitogen associated with angiogenesis (Lennmyr et al., 1998), as well as a potent mediator of vascular permeability (Senger et al., 1983). VEGF is reported to be involved in brain edema associated with tumors (Plate and Risau, 1995), cerebral infarction (Cobbs et al., 1998), and neurotrauma (Papavassiliou et al., 1997).

VEGF works through the activation of Src family kinases, that are located downstream in the VEGF signal transduction pathway (Eliceiri et al., 1999). Src family kinases mediate signaling in response to a variety of growth factors, including VEGF (Schlessinger, 2000), and they contribute to, among others, angiogenesis, stimulation of cell survival, and acceleration of vascular permeability.

The synthetic pyrazolopyrimidine, 4-amino-5-(4-methylphenyl)-7-(t-butyl)pyrazolo[3,4-d]pyrimidine (PP1) is a novel, potent, and selective inhibitor of Src family tyrosine kinases (Hanke et al., 1996). A recent study found that PP1 significantly reduced the size of infarction in a mouse middle cerebral artery (MCA) occlusion model (Paul et al., 2001).

On the basis of these findings, we hypothesized that the inhibition of Src family kinases by PP1 may lead to the reduction of edema formation and inflammatory responses caused by various forms of neurotrauma. In this study, we examined the effects of PP1 on vascular permeability and inflammatory responses in a rat spinal cord compression model.

## MATERIALS AND METHODS

### *Spinal Cord Compression Model*

All animal experiments were conducted in compliance with the *NIH Guide for the Care and Use of Laboratory Animals* (1996) and the *Osaka University Medical School Guidelines for the Care and Use of Laboratory Animals*. Surgical and experimental procedures were approved by the Osaka University Medical School Animal Care and Use Committee.

Forty female Wistar rats (age = 8 weeks, body weight = 200 g) were used for this model, because urinary management of female rats was considered easier than that of males. The rats were anesthetized with an intraperitoneal injection of pentobarbital (60 mg/kg) and placed in the prone position. A vertical linear incision was made along the midline of the back, followed by a single segmental laminectomy over Th10 to expose the dura of the spinal cord. A Sugita temporary clip with a calibrated closing force of 70 g (Mizuho Co., Ltd., Tokyo, Japan) was applied over the dura to compress the spinal cord for 3 sec. The skin was then closed and the animals were returned to their cages. During surgery, rectal temperature was maintained at ~36–37°C with a controlled heating pad.

PP1 (Biomol Research Laboratories, Plymouth Meeting, PA), suspended in 30% dimethyl sulfoxide (DMSO) with 0.01 M phosphate-buffered saline (PBS; He et al., 2000), was administered intraperitoneally 10 min after spinal cord compression (PP1 group) following the methods of Paul et al. (2001). The dosage used was 1.5 mg/kg weight to ensure that the maximum effect was achieved with this dosage (Paul et al., 2001). For the control group, the vehicle alone was administered using the same procedure.

### *Histological Procedure*

On days 1, 3, and 7 after compression, rats from the two groups were deeply anesthetized with an intraperitoneal injection of pentobarbital (100 mg/kg). Their spinal cords were rapidly removed and immediately covered with Tissue-Tek embedding medium (Sakura Finetek, Torrance, CA), frozen at −80°C in 2-methylbutane, and stored at that temperature until further processing. Sagittal serial cryostat sections were cut at a thickness of 10 $\mu$m and then processed for either hematoxylin and eosin (HE) staining or immunohistochemistry (Bartholdi et al., 1997).

HE staining was used to estimate the extent of the damage. With the use of Scion image analysis software for Windows (1998; Scion Corporation, Frederick, MD), the extent of contusional lesion on day 1 after compression was calculated as the area where the color intensity of eosin had decreased by more than 50% in sagittal sections containing the central canal. On days 3 and 7, the area of inflammatory cell infiltration around the contusional area was also included in the calculation of the contusion's extent. This measurement was performed for three consecutive sections from each rat.

### *Immunohistochemical Staining*

Immunohistochemical staining of VEGF, IgG, and ED-1 was performed to examine respectively, the expression of VEGF, the extent of edema, and the extent of macrophage infiltration. Immunohistochemical staining was done according to the method of Fujinaka et al. (2003), with some modifications.

Sections were fixed with 4% paraformaldehyde in 0.1 M phosphate buffer for 45 min, permeated with methanol at −20°C for 10 min, and finally incubated with 3% hydrogen peroxidase for 30 min to quench endogenous peroxidase. The sections were rinsed in PBS and nonspecific protein binding was blocked with 2% normal horse serum in a buffer (0.1% Triton X-100 and 5% sucrose in

PBS) for 20 min. Incubation with the primary antibodies was carried out at 4°C overnight.

The primary antibodies used for this procedure were anti-VEGF mouse monoclonal antibody (Santa Cruz Biotechnology, Santa Cruz, CA; diluted 1:100) and anti-ED-1 mouse monoclonal antibody (Serotec, Kidlington, Oxford, UK; diluted 1:100). To detect binding of the primary antibodies to the corresponding antigens, the sections were first incubated with the biotinylated anti-mouse IgG antibody (Vector Laboratories, Burlingame, CA; diluted 1:200) at room temperature for 30 min and then with abidin-biotin peroxidase complex (Vectastain Elite ABC kit, Vector Laboratories) for 30 min. The end product was visualized by means of a 3,3′-diamino-benzidine tetrahydrochloride (DAB) and hydrogen peroxidase solution and counterstained with hematoxylin. Control immunostaining consisted of the omission of the primary antibody from the immunostaining protocol.

The procedure for anti-IgG rabbit polyclonal antibody (Vector Laboratories; diluted 1:200) differed somewhat from the method described above in that the sections were incubated with 2% normal rabbit serum for 20 min, followed by incubation with this antibody at room temperature for 30 min, and finally with the abidin-biotin peroxidase complex for 30 min. The other procedures were the same as described above.

Scion image for Windows was used to define the extent of ED-1 positive cell infiltration as the area where more than 10 ED-1–positive cells were observed under high magnification (×400) in the sagittal section containing the central canal. These measurements were performed for three consecutive sections from each rat.

### *Determination of Water Content after Spinal Cord Compression*

As another method to assess edema, the spinal cords obtained on days 1, 3, and 7 after compression under deep anesthesia were cut into lengths of 3 cm in the rostrocaudal direction, centering to the compression site. The spinal cords of nonoperated, normal animals served as normal controls. The wet weight of the spinal cords was measured immediately after their removal, after which the cords were dried at 100°C for 72 h and their dry weight determined (Suzuki et al., 2002). The water content was calculated using the following equation: water content (%) = [(wet weight − dry weight)/wet weight] × 100 (Paczynski et al., 2000).

### *Quantification of TNFα and IL-1β mRNA Levels in the Injured Spinal Cord*

To investigate the magnitude of the inflammatory response, tumor necrosis factor a (TNFα) mRNA and interleukin 1β (IL-1β) mRNA expression were measured with a real-time polymerase chain reaction (RT-PCR) system. This technique facilitates the quantification of complementary DNA (cDNA) amplification and involves a fluorescence-based RT-PCR followed by measurement of the amplification with the ABI PRISM 7700 Sequence Detection System (Applied Biosystems, Foster, CA).

RT-PCR analysis was performed as reported elsewhere (Ueno et al., 2001). Briefly, total RNA was purified from 30 mg of each injured spinal cord obtained 6 h after compression using the RNA Easy Mini Kit (Qiagen, Hilden, Germany), according to the manufacturer's instructions. For this procedure, genomic DNA was dissolved by DNase I treatment and RNA samples were frozen in liquid nitrogen and stored at −80°C until use.

First-strand cDNA synthesis from the RNA samples was carried out using the SuperScript First-Strand Synthesis System for RT-PCR (Invitrogen Corp., Carlsbad, CA). cDNA synthesis was performed in triplicate, and for each cDNA synthesis, 200 ng of mRNA in 8 μL of water was incubated with 1 μL of oligo-d(T) primer (0.5 μg/μL) and 1 μL of dNTP mix (10 mM) at 65°C for 5 min. The solution was briefly chilled on ice, and then added to 2 μL of 10 × RT buffer, 4 μL of 25 mM $MgCl_2$, 2 μL of 0.1 M DTT, and 1 μL of RNase Out Recombinant RNase Inhibitor. After incubation at 42°C for 2 min, 1 μL (50 units) of SuperScript II reverse transcriptase was added to each tube. The reaction was incubated at 42°C for 60 min, followed by 70°C for 15 min to terminate the reaction. After the reactant had been collected by means of brief centrifugation, 1 μL of RNase H was added to each tube and incubated at 37°C for 20 min to dissolve the residual RNA. Parallel reactions for each RNA sample were run in the absence of SuperScript II reverse transcriptase to detect the presence of any contaminating genomic DNA (no RT samples). Following synthesis, cDNA was aliquoted into microtiter plates in preparation for TaqMan RT-PCR.

For each PCR, 1 μL of cDNA was used and each transcript was measured in triplicate. The RT-PCR technique is based on the hydrolysis of a specific fluorescent probe at each amplification cycle by the 5′-endonuclease activity of Taq polymerase. We used the technique as described by Depre et al. (1998) and Medhust et al. (2000), with some modifications. Predeveloped TaqMan Assay reagents (Applied Biosystems) were used for the probes and primers for TNFα and IL-1β in quantities of 200 nmol/L for each PCR as recommended by the manufacturer. PCR was then performed with 40 cycles of naturing at 95°C for 15 sec and annealing at 60°C for 1 min. Due to the relative lack of precision of spectrophotometric measurements of RNA concentration, the level of transcripts for the cellular enzyme glyceraldehyde 3-

phosphate dehydrogenase (GAPDH) was quantitatively measured in all samples as the internal control. The GAPDH primer and probe sequences were as follows: forward primer, CCATCACTGCCACTCAGAAGAC; reverse primer, TCATACTTGGCAGGTTTCTCCA; and probe, CGTGTTCCTACCCCCAATGTATCCGT.

All TaqMan RT-PCR data was captured with Sequence Detector Software (SDS version 1.7; PE Applied Biosystems, Weiterstadt, Germany). The mRNA/GAPDH value for each sample was calculated, followed by calculation of the induction value for comparison with the normal rat mRNA/GAPDH level.

### *Statistical Analysis*

Data are expressed as mean ± standard deviation (SD). The Mann-Whitney *U* test was performed using Stat View (Version 4, SAS Institute, Cary, NC) for comparisons of the control and PP1 groups. The *p*-values of $<0.05$ were considered significant.

## RESULTS

### *Extent of Contusional Lesions*

After recovery from anesthesia, all animals were paraplegic. HE-stained sections demonstrated that on day 1 the location of the contusional lesions coincided with the location of the compression. On days 3 and 7, inflammatory cells had infiltrated the area of the contusion and its immediate surround. The areas of the contusional lesions of the control group measured 5.56 ± 1.29 $mm^2$ ($n = 14$) and of the PP1 group 5.50 ± 1.19 $mm^2$ ($n = 12$) on day 1. Because there was no significant difference, it was assumed that the severity of the primary damage was essentially the same in both groups. On day 3, however, the injured areas of the control group and the PP1 group were 7.79 ± 3.32 $mm^2$ ($n = 16$) and 5.06 ± 1.19 $mm^2$ ($n = 16$), respectively, showing a significant reduction (approximately 35%) in the PP1 group compared to the control group ($p < 0.01$). Although the areas of the contusional lesions of both groups were reduced on day 7 as compared to day 3, they showed the same pattern as that reported on day 3 (data not shown).

### *VEGF Expression*

On days 3 and 7 after compression, marked VEGF protein expression was detected in the neurons and glial cells surrounding the contusional lesion in both the control and PP1 groups. This expression was most intense on day 3. There was no significant difference between the two groups in terms of VEGF expression (Fig. 1).

### *Extent of Edema*

The extent of edema was investigated first with the aid of the anti-IgG antibody. The area of edema of the PP1 group on day 1 after compression was considerably reduced compared with that of the control group (Fig. 2). The water content of the spinal cord on days 1, 3, and 7 is shown in Figure 3. The water content was 66.86 ± 1.78% in nonoperated normal animals ($n = 6$). Spinal cord compression increased the water content to 71.81 ± 1.31% on day 1 after compression (control group, $n = 6$) whereas those rats administered PP1 had a water content of 70.06 ± 0.45% (PP1 group, $n = 6$). On day 3, the water content in the control group was 74.66 ± 1.54% ($n = 4$) and 72.23 ± 0.60% ($n = 4$) in the PP1 group, indicating that, compared with day 1, edema was aggravated in both groups. On day 7, however, the corresponding values were 70.73 ± 0.32% ($n = 5$) and 69.75 ± 0.50% ($n = 4$), showing that in both groups edema was reduced compared with day 3 values. On days 1, 3, and 7, the *p*-values were 0.0163, 0.0202, and 0.0127, respectively, indicating a statistically significant difference between the two groups.

### *Macrophage Infiltration*

Macrophages infiltration was investigated with the aid of anti-ED-1 antibody. On day 1 only a few ED-1–positive cells existed in the contusional lesions of both groups. On day 3, ED-1–positive cells had infiltrated extensively in the control group, but in the PP1 group they were restricted to the contusional lesion and its immediate surround (Fig. 4). The areas infiltrated by ED-1–positive cells in the control and PP1 groups were 10.52 ± 5.50 $mm^2$ ($n = 10$) and 4.07 ± 0.80 $mm^2$ ($n = 10$), respectively ($p < 0.005$); that is, the area of macrophage infiltration was significantly (approximately 60%) smaller in the PP1 group than in the control group. On day 7, the amount of macrophage infiltration was similar to that seen on day 3, but the area infiltrated by ED-1 positive cells in the control group was 7.95 ± 0.60 $mm^2$ ($n = 6$), which was smaller than on day 3. The area in the PP1 group on day 7 was 4.08 ± 0.15 $mm^2$ ($n = 6$), showing a significant difference between the two groups ($p < 0.005$; Fig. 5).

### *TNFα and IL-1β mRNA Expressions in the Injured Spinal Cord*

In the control group, the fold-induction rate of expression of the gene encoding TNFα at 6 h after compression was 89.96 ± 53.23 ($n = 6$) compared with that seen in normal rats. In the PP1 group, however, the fold induction was significantly reduced to 42.00 ± 18.09 ($p < 0.005$, $n = 6$; Fig. 6a). The fold-induction rate of

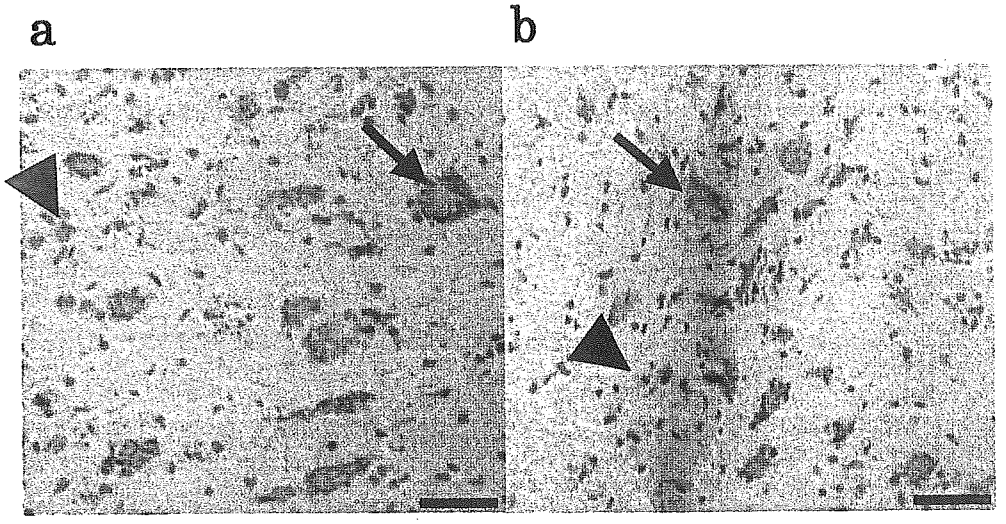


**FIG. 1.** Photomicrographs of VEGF immunohistochemical examination on day 3 after compression in the control group (**a**) and the PP1 group (**b**). VEGF protein expression was detected in the neurons (arrows) and glial cells (arrowheads) around the contusion in both groups. There was no statistical difference between the control and PP1 groups. Bar = 50 $\mu$m.

IL-1$\beta$ mRNA expression at 6 h after compression was 288.19 $\pm$ 150.16 ($n$ = 8) for the control group and 191.81 $\pm$ 79.90 ($n$ = 8) for the PP1 group, a statistically significant difference ($p < 0.05$; Fig. 6b). These findings demonstrate that the expression of these genes was suppressed effectively by the administration of PP1.

## DISCUSSION

Neurological deficits as a result of spinal cord trauma are due to both primary and secondary damage. Primary damage is primarily the result of direct mechanical injury to the spinal cord parenchyma as a, whereas secondary

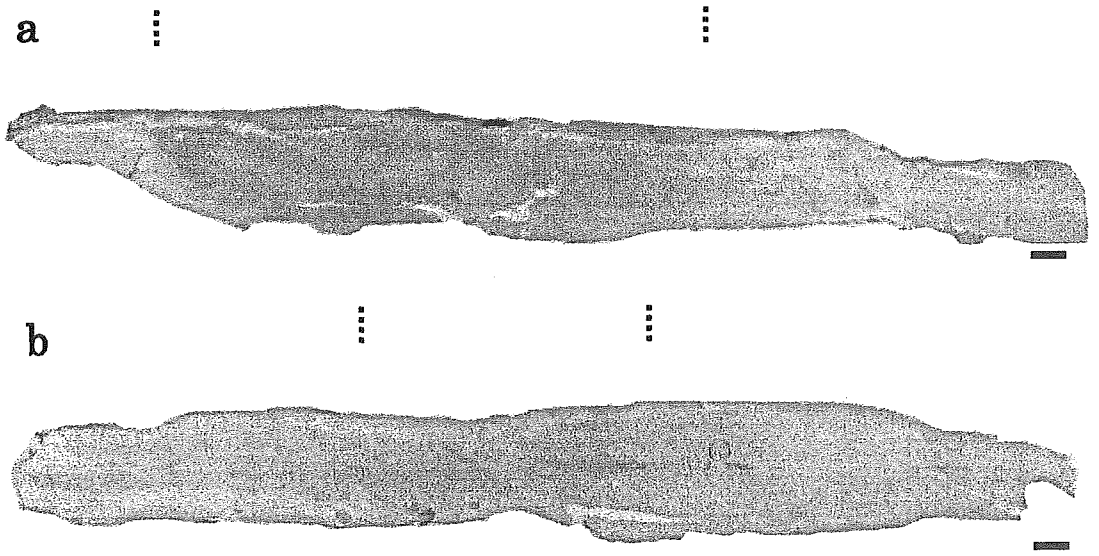


**FIG. 2.** Photomicrographs of anti-rat IgG immunohistochemical examination on day 1 after compression in the control group (**a**) and the PP1 group (**b**). Extent of edema (area between dotted lines), positive for IgG, was much less in the PP1 group than in the control group. Bar = 1 mm.

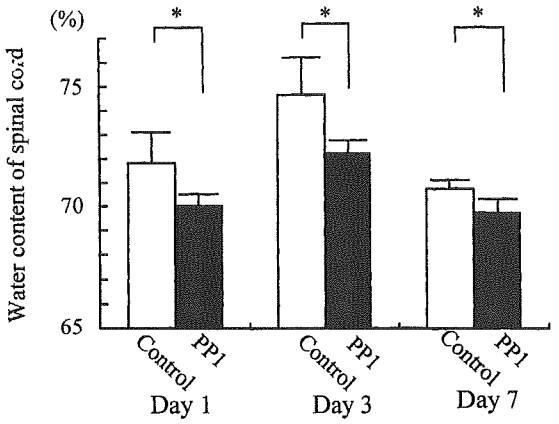


**FIG. 3.** Water content of the spinal cord in the control group and the PP1 group on days 1, 3, and 7 after compression. Values represent mean ± SD. Administration of PP1 significantly reduced the water content measured on all days ($*p < 0.05$).

damage may be initiated, for example, by an increase in vascular permeability, an increased inflammatory response, ischemia, excitatory amino acids, and free radicals (Ghirnikar et al., 2001; Topsakal et al., 2002). This study demonstrated that PP1 given 10 min after injury could reduce edema, the contusional area, macrophage infiltration, and inflammatory mediators after spinal cord compression injury in rats. The findings obtained with HE staining demonstrated that, although in both groups the severity of primary damage was virtually the same, in the control group the contusional area increased with time however, in contrast, PP1 attenuated this increase. Thus, PP1 can reduce secondary damage after spinal cord injury.

Similar levels of VEGF expression were observed in both the control and PP1 groups. Accordingly, Our results suggest that PP1 administration did not affect VEGF expression, which is consistent with the findings of a permanent MCA occlusion model (Kovács et al., 1996; Lennmyr et al., 1998) and a cerebral cold injury model (Nag et al., 1997). Moreover, the edema formation in our study indicated that the water content of the injured spinal cord peaked on day 3 in both groups and was reduced significantly by PP1 administration. Paul et al. (2001) reported that Src-deficient mice showed negligible vascular permeability in response to VEGF and were protected from edema-associated damage following stroke. Thus, Src may play a key role in VEGF-mediated edema formation.

In our opinion, VEGF may also contribute to edema formation in spinal cord injury, and the following mechanisms may be involved in this process. VEGF-induced stimulation of VEGF receptors (VEGFR) leads to the recruitment of Src and stimulation of its catalytic activity. Src is then activated by binding of the Src homology 2 domain to a tyrosine autophosphorylation site on VEGFR, and the activated Src may feed into a similar signaling pathway composed of phosphatidylinositol 3-kinase (PI-3K), phosphoinositide-dependent protein kinase (PDK), and Akt, leading to stimulation of endothelial cell survival, angiogenesis, and edema formation (Schlessinger, 2000). PP1, a widely applied, potent, and selective inhibitor of Src family tyrosine kinases, exerts its function by decreasing the phosphorylation of Src at $Tyr^{416}$, a known site of autophosphorylation (Hunter, 1987). Therefore, the mechanism of edema reduction observed in our study may be due to the suppression of Src family kinase function by PP1 after spinal cord injury.

Akt signaling mediates VEGF-induced vascular permeability (Six et al., 2002). The serine protein kinase Akt, that is located downstream of Src, is activated by PI-3K

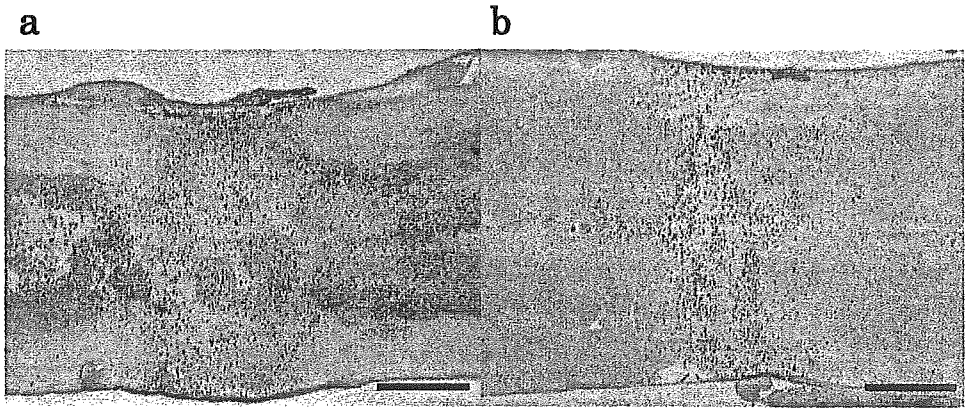


**FIG. 4.** Photomicrographs of ED-1 immunohistochemical examination on day 3 after compression in the control group (**a**) and the PP1 group (**b**). Abundant ED-1 positive cells were seen in the control group, but in the PP1 group they were restricted to the contusional area and its immediate surroundings. Bar = 1 mm.

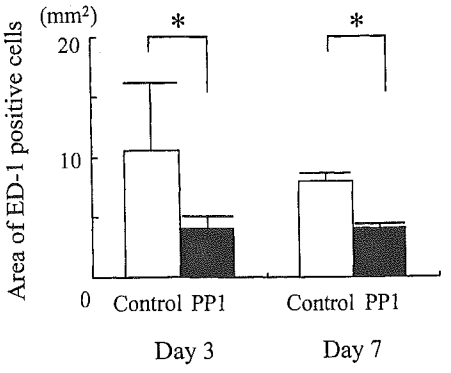


**FIG. 5.** Areas of ED-1 positive cell infiltration in the control group and the PP1 group on days 3 and 7 after compression. Values represent mean ± SD. The area of the ED-1 positive cell infiltration in the PP1 group was significantly smaller compared with that in the control group ($*p < 0.005$).

and promotes cell survival, angiogenesis, and vascular remodeling by mediating nitric oxide (NO) production (Fujio and Walsh, 1999; Fulton et al., 1999). Furthermore, PP1 may be involved in the PI-3K/Akt/NO pathway (Radisavljevic et al., 2000).

The area infiltrated by macrophages in our study peaked on day 3 in the control group. The administration of PP1 suppressed the infiltration of macrophages and restricted them to the area of the contusion and its immediate surround on days 3 and 7. Because PP1 reduced the extent of macrophage infiltration more dramatically than that of edema, it appears that reduction of inflammatory cells may be particularly important for neuroprotection.

PP1 inhibits the production of TNF$\alpha$, IL-1$\beta$, and inducible NO synthase (iNOS) in murine macrophages stimulated with lipopolysaccharide (LPS) and interferon $\gamma$ (IFN$\gamma$) (Orlicek et al., 1999; Lin et al., 2000). Macrophages and monocytes contain three major Src family kinases: Hck, Lyn, and Fgr (Meng and Lowell, 1997). Moreover, PP1 has been shown to inhibit Lyn with an $IC_{50}$ approximately 30-fold lower than that of Src (Shah et al., 2002). It is therefore possible that, because PP1 blocks the activity of macrophages more strongly through the inhibition of Lyn, the overall inflammation response and the chemotaxis of macrophages are suppressed more strongly than edema formation.

Our study also demonstrated that PP1 suppressed the expression of TNF$\alpha$ and IL-1$\beta$ mRNA in the injured spinal cord. These findings support the concept that the administration of PP1 effectively blocks gene expression related to early inflammatory response in spinal cord injury (Bartholdi and Schwab, 1997; Dinkel et al., 2003). In addition, PP1 may block the activity of Src family kinases to suppress macrophage activities that produce these cytokines, although we could not identify the cellular origins of TNF$\alpha$ and IL-1$\beta$.

Our results provide histological evidence that PP1 reduces secondary damage. The optimal timing and dosing of PP1 remain to be determined by evaluating both the histological and neurological effects of its administration. It's adverse effects must also be thoroughly investigated before considering the use of PP1 for the treatment of human spinal cord injury.

## ACKNOWLEDGMENTS

We thank Dr. Shayne Morris, Department of Neurosurgery, Yukioka Hospital, for his very helpful advice and comments.

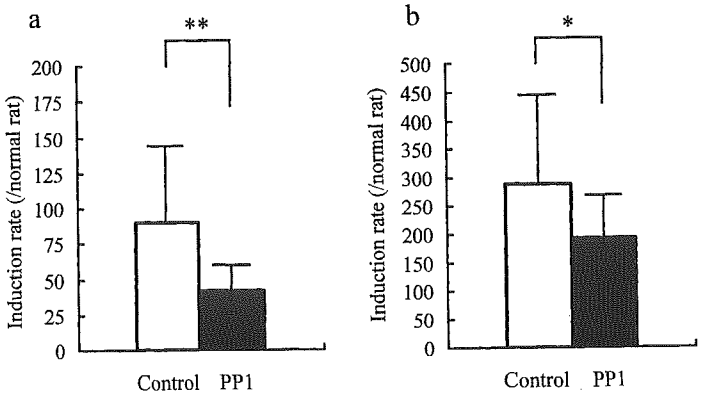


**FIG. 6.** Induction rate of mRNA in the rat spinal cord 6 h after compression: (**a**) TNF$\alpha$ mRNA and (**b**) IL-1$\beta$ mRNA. The level of the mRNAs in these samples was normalized to the mRNA level of GAPDH, and the induction rates were calculated by comparing them with the levels in normal rat spinal cord. Values represent mean ± SD. PP1 significantly suppressed both TNF$\alpha$ and IL-1$\beta$ mRNA ($*p < 0.05$, $**p < 0.005$).

## REFERENCES


BARTHOLDI, D., and SCHWAB, M.E. (1997). Expression of pro-inflammatory cytokine and chemokine mRNA upon experimental spinal cord injury in mouse: an *in situ* hybridization study. Eur. J. Neurosci. **9,** 1422–1438.

BARTHOLDI, D., RUBIN, B.P., and SCHWAB, M.E. (1997). VEGF mRNA induction correlates with changes in the vascular architecture upon spinal cord damage in the rat. Eur. J. Neurosci. **9,** 2549–2560.

COBBS, C.S., CHEN, J., GREENBERG, D.A., et al. (1998). Vascular endothelial growth factor expression in transient focal cerebral ischemia in the rat. Neurosci. Lett. **249,** 79–82.

DEPRE, C., SHIPLEY, G.L., CHEN, W., et al. (1998). Unloaded heart in vivo replicates fetal gene expression of cardiac hypertrophy. Nat. Med. **4,** 1269–1275.

DINKEL, K., MACPHERSON, A., and SAPOLSKY, R.M. (2003). Novel glucocorticoid effects on acute inflammation in the CNS. J. Neurochem. **84,** 705–716.

EARNHARDT, J.N., STREIT, W.J., ANDERSON, D.K., et al. (2002). Induction of manganese superoxide dismutase in acute spinal cord injury. J. Neurotrauma **19,** 1065–1079.

ELICEIRI, B.P., PAUL, R., SCHWARTZBERG, P.L., et al. (1999). Selective requirement of Src kinases during VEGF-induced angiogenesis and vascular permeability. Mol. Cell **4,** 915–924.

FUJINAKA, T., KOHMURA, E., YUGUCHI, T., et al. (2003). The morphological and neurochemical effects of diffuse brain injury on rat central noradrenergic system. Neurol. Res. **25,** 35–41.

FUJIO, Y., and WALSH, K. (1999). Akt mediates cytoprotection of endothelial cells by vascular endothelial growth factor in an anchorage-dependent manner. J. Biol. Chem. **274,** 16349–16354.

FULTON, D., GRATTON, J.-P., McCABE, T.J., et al. (1999). Regulation of endothelium- derived nitric oxide production by the protein kinase Akt. Nature **399,** 597–601.

GHIRNIKAR, R.S., LEE, Y.L., and ENG, L.F. (2001). Chemokine antagonist infusion promotes axonal sparing after spinal cord contusion injury in rat. J. Neurosci. Res. **64,** 582–589.

HANKE, J.H., GARDNER, J.P., DOW, R.L., et al. (1996). Discovery of a novel, potent, and Src family-selective tyrosine kinase inhibitor. J. Biol. Chem. **271,** 695–701.

HE, H., HIROKAWA, Y., LEVITZKI, A., et al. (2000). An Anti-Ras cancer potential of PP1, an inhibitor specific for Src family kinases: *in vitro* and *in vivo* studies. Cancer J. **6,** 243–248.

HUNTER, T. (1987). A tail of two src's: mutatis mutandis. Cell **49,** 1–4.

KOVÁCS, Z., IKEZAKI, K., SAMOTO, K., et al. (1996). VEGF and flt expression time kinetics in rat brain infarct. Stroke **27,** 1865–1873.

LENNMYR, F., ATA, K.A., FUNA, K., et al. (1998). Expression of vascular endothelial growth factor (VEGF) and its receptors (Flt-1 and Flk-1) following permanent and transient occlusion of the middle cerebral artery in the rat. J. Neuropathol. Exp. Neurol. **57,** 874–882.

LIN, T., HIRJI, N., STENTON, G.R., et al. (2000). Activation of Macrophage CD8: pharmacological studies of TNF and IL-1$\beta$ production. J. Immunol. **164,** 1783–1792.

MEDHURST, A.D., HARRISON D.C., READ S.J., et al. (2000). The use of TaqMan RT-PCR assays for semiquantitative analysis of gene expression in CNS tissue and disease models. J. Neurosci. Met. **98,** 9–20.

MENG, F., and LOWELL, C.A. (1997). Lipopolysaccharide (LPS)-induced macrophage activation and signal transduction in the absence of Src-family kinases Hck, Fgr, and Lyn. J. Exp. Med. **185,** 1661–1670.

NAG, S., TAKAHASHI, J.L., KILTY, D.W., et al. (1997). Role of vascular endothelial growth factor in blood–brain barrier breakdown and angiogenesis in brain trauma. J. Neuropathol. Exp. Neurol. **56,** 912–921.

ORLICEK, S.L., HANKE, J.H., and ENGLISH, B.K. (1999). The Src family-selective tyrosine kinase inhibitor PP1 blocks LSP and IFN-gamma-mediated TNF and iNOS production in murine macrophages. Shock **12,** 350–354.

PACZYNSKI, R.P., VENKATESAN, R., DIRINGER, M.N., et al. (2000). Effects of fluid management on edema volume and midline shift in a rat model of ischemic stroke. Stroke **31,** 1702–1708.

PAPAVASSILIOU, E., GOGATE, N., PROESCHOLDT, M., et al. (1997). Vascular endothelial growth factor (vascular permeability factor) expression in injured rat brain. J. Neurosci. Res. **49,** 451–460.

PAUL, R., ZHANG, Z.G., ELICEIRI, B.P., et al. (2001). Src deficiency or blockade of Src activity in mice provides cerebral protection following stroke. Nat. Med. **7,** 222–227.

PLATE, K.H., and RISAU, W. (1995). Angiogenesis in malignant gliomas. Glia **15,** 339–347.

RADISAVLJEVIC, Z., AVRAHAM, H., and AVRAHAM, S. (2000). Vascular endothelial growth factor up-regulates ICAM-1 expression via the phosphatidylinositol 3 OH-kinase/AKT/nitric oxide pathway and modulates migration of brain microvascular endothelial cells. J. Biol. Chem. **275,** 20770–20774.

SCHLESSINGER, J. (2000). New role for Src kinases in control of cell survival and angiogenesis. Cell **100,** 293–296.

SENGER, D.R., GALLI, S.J., DVORAK, A.M., et al. (1983). Tumor cells secrete a vascular permeability factor that promotes accumulation of ascites fluid. Science **219,** 983–985.

SHAH, O.J., KIMBALL, S.R., and JEFFERSON, L.S. (2002).

The Src-family tyrosine kinase inhibitor PP1 interferes with the activation of ribosomal protein S6 kinases. Biochem. J. **366,** 57–62.

SIX, I., KUREISHI, Y., LUO, Z., et al. (2002). Akt signaling mediates VEGF/VPF vascular permeability *in vivo*. FEBS. Lett. **532,** 67–69.

SKÖLD, M., CULLHEIM, S., HAMMARBERG, H., et al. (2000). Induction of VEGF and VEGF receptors in the spinal cord after mechanical spinal injury and prostaglandin administration. Eur. J. Neurosci. **12,** 3675–3686.

SUZUKI, Y., MATSUMOTO, Y., IKEDA, Y., et al. (2002). SM-20220, a $Na^+/H^+$ exchanger inhibitor: effects on ischemic brain damage through edema and neutrophil accumulation in rat middle cerebral artery occlusion model. Brain. Res. **945,** 242–248.

TOPSAKAL, C., EROL, F.S., OZVEREN, M.F., et al. (2002). Effects of methylprednisolone and dextromethorphan on lipid peroxidation in an experimental model of spinal cord injury. Neurosurg. Rev. **25,** 258–266.

UENO, T., SAWA, Y., KITAGAWA-SAKAKIDA, S., et al. (2001). Nuclear factor-κB decoy attenuates neuronal damage after global brain ischemia: a future strategy for brain protection during circulatory arrest. J. Thorac. Cardiovasc. Surg. **122,** 720–727.

Address reprint requests to:
*Takamichi Yuguchi, M.D., Ph.D.*
*Department of Neurosurgery*
*Spine and Spinal Cord Center*
*Yukioka Hospital*
*2-2-3 Ukita Kita-ku*
*Osaka City, Osaka 530-0021, Japan*

*E-mail:* yuguchi@yukioka.or.jp

J Neurosurg 99:47–51, 2003

# Efficacy of moderate hypothermia in patients with severe head injury and intracranial hypertension refractory to mild hypothermia

TADAHIKO SHIOZAKI, M.D., PH.D., YOSHIKAZU NAKAJIMA, M.D., PH.D., MAMORU TANEDA, M.D., PH.D., OSAMU TASAKI, M.D., PH.D., YOSHIAKI INOUE, M.D., HITOSHI IKEGAWA, M.D., ASAKO MATSUSHIMA, M.D., HIROSHI TANAKA, M.D., PH.D., TAKESHI SHIMAZU, M.D., PH.D., AND HISASHI SUGIMOTO, M.D., PH.D.

*Departments of Traumatology and Neurosurgery, Osaka University Graduate School of Medicine; and Department of Neurosurgery, Kinki University School of Medicine, Osaka, Japan*

*Object.* This study was performed to determine whether moderate hypothermia (31°C) improves clinical outcome in severely head injured patients whose intracranial hypertension cannot be controlled using mild hypothermia (34°C).

*Methods.* Twenty-two consecutive severely head injured patients who fulfilled the following criteria were included in this study: an intracranial pressure (ICP) that remained higher than 40 mm Hg despite the use of mild hypothermia combined with conventional therapies; and a Glasgow Coma Scale score of 8 or less on admission. After the failure of mild hypothermia in combination with conventional therapies; patients were exposed to moderate hypothermia as quickly as possible. As brain temperature was reduced from 34 to 31°C, the volume of intravenous fluid infusion was increased significantly from 1.9 ± 0.9 to 2.6 ± 1.2 mg/kg/hr ($p < 0.01$), and the dose of dopamine infusion increased significantly from 4.3 ± 3.1 to 8.2 ± 4.4 μg/kg/min ($p < 0.01$). Nevertheless, mean arterial blood pressure and heart rate decreased significantly from 97.1 ± 13.1 to 85.1 ± 10.5 mm Hg ($p < 0.01$) and from 92.2 ± 13.8 to 72.2 ± 14.3 beats/minute at ($p < 0.01$) at 34 and 31°C, respectively. Arterial base excess was significantly aggravated from −3.3 ± 4 at 34°C to −5.6 ± 5.4 mEq/L (at 31°C; $p < 0.05$). Likewise, serum potassium concentration, white blood cell counts, and platelet counts at 31°C decreased significantly compared with those at 34°C ($p < 0.01$).

In 19 (86%) of 22 patients, elevation of ICP could not be prevented using moderate hypothermia. In the remaining three patients, ICP was maintained below 40 mm Hg by inducing moderate hypothermia; however, these three patients died of multiple organ failure. These results clearly indicate that moderate hypothermia induces complications more severe than those induced by mild hypothermia without improving outcomes.

*Conclusions.* The authors concluded that moderate hypothermia is not effective in improving clinical outcomes in severely head injured patients whose ICP remains higher than 40 mm Hg after treatment with mild hypothermia combined with conventional therapies.

KEY WORDS • **head injury** • **intracranial pressure** • **hypothermia**

We have reported that mild hypothermia (34°C) is effective in preventing the elevation of ICP in severely head injured patients whose ICP remains higher than 20 mm Hg but lower than 40 mm Hg after undergoing conventional therapies.[14,15] Our findings are consistent with those of other investigators: mild hypothermia significantly reduces high ICP in patients with severe head injury.[7,11] Even in the National Acute Brain Injury Study, Clifton, et al.,[3] mentioned that mild hypothermia reduced elevated ICP. Nevertheless, they concluded that mild hypothermia was not effective in improving outcomes in patients with severe head injury. The body temperature that is most effective for controlling refractory intracranial hypertension in severely head injured patients has yet to be defined. Klementavicius, et al.,[8] demonstrated in the rat that CBF and $CMRO_2$ were exponentially reduced as temperature decreased from 38 to 30°C (see Fig. 1 in their report). With intact coupling of CBF and $CMRO_2$, Todd and Weeks[17] showed in the rat that metabolic suppression led to a drop in ICP. It would therefore be expected that a further decrease in brain temperature would cause a further reduction in ICP. Our aim was to determine whether the same results could be expected in the clinical setting. In the present study, we prospectively assessed the efficacy and safety of moderate hypothermia (31°C) in the treatment of severely head injured patients in whom ICP could not be maintained at a level lower than 40 mm Hg despite the use of mild hypothermia (34°C).

*Abbreviations used in this paper:* CBF = cerebral blood flow; $CMRO_2$ = cerebral metabolic rate of oxygen; CPP = cerebral perfusion pressure; CSF = cerebrospinal fluid; CT = computerized tomography; ICP = intracranial pressure; MABP = mean arterial blood pressure; WBC = white blood cell.

## Clinical Material and Methods

### *Patient Population*

Between January 1998 and July 2002, a total of 124 severely head injured patients were admitted to the Department of Traumatology at the Osaka University Hospital.